Chemical Geology 470 (2017) 132–140

Contents lists available at ScienceDirect

Chemical Geology

journal homepage: www.elsevier.com/locate/chemgeo

Adsorption isotherm, mechanism, and geometry of Pb(II) on magnetites substituted with transition metals

Xiaoliang Liang[a], Gaoling Wei[b], Juan Xiong[d], Fuding Tan[a,c], Hongping He[a,*], Chenchen Qu[d], Hui Yin[d], Jianxi Zhu[a], Runliang Zhu[a], Zonghua Qin[e], Jing Zhang[f]

[a] CAS Key Laboratory of Mineralogy and Metallogeny and Guangdong Provincial Key Laboratory of Mineral Physics and Materials, Guangzhou Institute of Geochemistry, Chinese Academy of Sciences, Guangzhou 510640, PR China
[b] Guangdong Key Laboratory of Integrated Agro-Environmental Pollution Control and Management, Guangdong Institute of Eco-Environmental Science & Technology, Guangzhou 510650, PR China
[c] University of Chinese Academy of Sciences, Beijing 100049, PR China
[d] Key Laboratory of Arable Land Conservation (Middle and Lower Reaches of Yangtse River) Ministry of Agriculture, College of Resources and Environment, Huazhong Agricultural University, Wuhan 430070, PR China
[e] State Key Laboratory of Ore Deposit Geochemistry, Institute of Geochemistry, Chinese Academy of Sciences, Guiyang 550081, PR China
[f] Beijing Synchrotron Radiation Facility, Institute of High Energy Physics, Chinese Academy of Sciences, Beijing 100039, PR China

ARTICLE INFO

Keywords:
Magnetite
Pb(II) adsorption
Acid-base titration
Adsorption geometry
XAFS

ABSTRACT

Iron oxides are abundant in natural waters and soils and have high capacities for scavenging Pb(II) by adsorption, which affects the transport and fate of Pb on the earth's surface. We investigated the adsorption of Pb (II) on magnetites substituted with commonly incorporated transition metals such as Cr, Mn, Co, and Ni. The adsorption capacity, mechanism, and local coordination of Pb(II) were investigated by traditional macroscopic studies, i.e., acid-base titration and batch adsorption experiment, complemented with X-ray absorption fine structure (XAFS) spectrum analysis and surface complexation model (SCM). The substitution increased the surface site density, while pH_{pzc} did not vary. Pb(II) adsorption was not suppressed by the presence of background electrolyte and improved as pH increased. The isotherms were well fit to the Langmuir adsorption model. The XAFS analysis demonstrated that Pb(II) ions were adsorbed on magnetite surface predominantly via inner-sphere complexation, where the adsorbed Pb(II) species was in bidentate binuclear corner-sharing geometry, independent of the adsorption capacity. This adsorption geometry can be applied to fit the experimental adsorption data well with the diffuse layer model (DLM). The substitutions improved the adsorption capacity in the following order: Cr > Ni > Mn > Co, and were discussed regarding the measured values of active site density and local coordination of adsorbed Pb(II). This study is the first documentation of Pb(II) adsorption on magnetite with different substitutions. The obtained results are of great significance for the understanding of Pb(II) surface complexation reactions on magnetite surface.

1. Introduction

Lead (Pb) contamination in soil, aquifer and surface water is a widespread and serious environmental problem. Effluents from the manufacture of storage batteries, paint and munitions, petroleum refining, and lead mine drainage are the main sources of Pb in the environment (Wang et al., 2010). Pb contamination is also caused by mineral resource development and sulfide mineral deposits (Mason et al., 2009). Pb and its compounds can accumulate in the body, resulting in severe hazards to human health, e.g., mental deficiency, anemia, anorexia, vomiting, and damage to the brain and nervous systems (Reich et al., 2010; Ma et al., 2015). Pb has been considered a priority metal of public health significance, due to its persistence, toxicity, and bioaccumulation characteristics (Arce et al., 2015). Understanding the transport and fate of Pb on the earth's surface and developing efficient technologies to passivate or inactivate Pb species in the contaminated environments are crucial.

The mineral solid-water interface plays a central role in regulating the Pb species and concentration in natural aqueous systems, thus affecting its mobility and bioavailability (Villalobos and Perez-Gallegos, 2008). Iron oxides are ubiquitous in soil and aquatic sediment as discrete particles, colloids, or coatings on other minerals, and have high capacities for scavenging dissolved metal ions such as Pb(II) by adsorption (Bargar et al., 1997). Secondary oxides in soil and sediments

* Corresponding author.
E-mail address: hehp@gig.ac.cn (H. He).

http://dx.doi.org/10.1016/j.chemgeo.2017.09.003
Received 13 July 2016; Received in revised form 29 August 2017; Accepted 6 September 2017
Available online 09 September 2017

have been considered the main contributors to Pb adsorption. Hematite and goethite are the most abundant iron oxides in the terrestrial surface environment with high aptitudes for Pb species scavenging, as confirmed by macroscopic, spectroscopic, and modeling studies. The effects of various environmental parameters such as residence time, pH, ionic strength, and temperature on the adsorption behavior of Pb(II) have been extensively studied (Zhao et al., 2011). Residence times, distribution of Pb(II) species (the most stable oxidation state of Pb in natural water), and adsorption density are vital to Pb adsorption/desorption behavior (Coston et al., 1995; Eick et al., 1999). Pb(II) is adsorbed as mononuclear bidentate complexes to the edges of FeO_6 octahedra in both goethite and hematite (Bargar et al., 1997). The adsorption geometries on goethite change with adsorption density from bidentate corner-sharing complexes to bidentate edge-sharing complexes (Templeton et al., 2003). The effects of inorganic ligands (e.g., sulfate (Elzinga et al., 2001), carbonate (Villalobos et al., 2001), chlorophyll (Bargar et al., 1998)), natural organic matter (e.g., humic acid (Orsetti et al., 2006) and citric acid (Perelomov et al., 2011)), and coexisting metal cations (e.g., Cd(II), Cu(II), and Zn(II) (Christophi and Axe, 2000)) on Pb adsorption were investigated. While less abundant than goethite and hematite in the soil, maghemite is a secondary iron oxide and common weathering product in temperate, tropical, and subtropical climatic regions. Maghemite displays superior adsorption to Pb(II) by forming inner-sphere complexes (Komarek et al., 2015). The adsorption properties of magnetite as a primary mineral for Pb(II) remain largely unknown, compared to other iron oxide minerals. However, magnetite is also a common constituent of soil and sediment, formed naturally via several pathways including iron metal corrosion, ferrous iron oxidation, and chemical and biological reduction of ferric oxides (Gorski et al., 2010). Additionally, nanomagnetite is the oxidation product of nano Fe^0, an emerging amendment that is being increasingly used for the remediation of contaminated groundwater and soil (Filip et al., 2014). Magnetite has been efficiently applied to remove toxic metals, including Cr(VI) (Zhang et al., 2017), Hg(II) (Wiatrowski et al., 2009), As(V) (Zhang et al., 2011), and U(VI) (Scott et al., 2005). The role of magnetite in the transport of Pb(II) on the earth's surface and the reaction mechanism is undeniable.

In most natural cases, lattice Fe cations in the magnetite structure can be substituted by transition metals, e.g., Ti^{4+}, V^{3+}, Mn^{2+}, Co^{2+}, Cr^{3+}, and Ni^{2+}. This interesting feature modifies the surface physicochemical properties of magnetite to different extents and is promising for the removal of heavy metals. Our previous study showed that Mn substitution in magnetite increases the surficial hydroxyl density and improves the adsorption properties for Pb(II) (Liang et al., 2014). However, the adsorption mechanism and morphology of Pb(II) species on the magnetite surface are still ambiguous. Other transition metals such as Co^{2+}, Cr^{3+}, and Ni^{2+} also change the surface properties of magnetite. For example, substitutions with Cr^{3+} and Ni^{2+} increase the surficial hydroxyl density and specific surface area (Liang et al., 2013), while Co^{2+} negatively affects the specific surface area (Wei et al., 2015). These variations should distinctly change the adsorption properties of magnetite towards Pb(II). Few studies have compared the effects of substituting these metals on the adsorption properties of magnetite.

The adsorption properties of magnetites with substitution of transition metals Cr, Mn, Co, and Ni towards Pb(II) cations were investigated with macroscopic and spectroscopic methods and surface complexation model (SCM). Our objectives were as follows: i) analyze the surface properties of substituted magnetites; ii) apply the substituted magnetites to Pb(II) adsorption and compare their adsorption capacity; iii) explore the effects of pH, ionic concentration, and Pb(II) concentration on the adsorption performance; and iv) discuss the adsorption mechanism and morphology of Pb(II) on magnetite. This study will help in greatly improving the understanding of the functional mechanism of magnetite-group minerals for the attenuation of heavy metals and for managing the fate of Pb(II) in the soil and aquatic environments.

2. Experimental

2.1. Magnetite preparation

All the chemicals and reagents used in this study were of analytical grade and used as received. Deionized water with a resistivity of 18.25 MΩ cm^{-1} at 25 °C was utilized for solution preparation, sample synthesis, and adsorption experiments. The magnetite samples were synthesized by a precipitation-oxidation method, as described previously (Liang et al., 2013). In brief, 0.90 mol L^{-1} $FeSO_4·7H_2O$ was dissolved in a HCl solution. Then, 1.0 mL of hydrazine was added to prevent ferrous oxidation; the pH was acidic enough (pH < 1) to prevent hydroxide precipitation. This solution was heated to 90–100 °C. An equal volume of a solution containing 4.0 mol L^{-1} NaOH and 0.90 mol L^{-1} $NaNO_3$ was added dropwise (10 mL min^{-1}) into the heated iron solution, and the reaction solution was maintained at 90 °C for 2 h while stirring at RCF 7. The solution was cooled to room temperature. It is necessary to emphasize that during the reaction, N_2 flux was passed through the solution to prevent ferrous oxidation. The particles were then separated by centrifugation at RCF 2301 for 5 min and washed with boiling distilled water, followed by another centrifugation. After 3–4 washings, the particles were collected and dried in vacuum at 100 °C for 24 h. The obtained sample was Fe_3O_4. The substituted magnetites containing Cr, Mn, Co, and Ni were prepared by following the steps mentioned above, except dissolving a certain amount of $CrCl_3·6H_2O$, $MnSO_4·H_2O$, $CoCl_2·6H_2O$, or $NiSO_4·6H_2O$ with $FeSO_4·7H_2O$ while preparing the acidic solution. The molar ratio of substituting metals (M) and Fe was controlled at 1:2. The total concentration of M and Fe was maintained at 0.90 mol L^{-1}. Based on the chemical composition obtained by ICP-AES analysis, the prepared magnetites were Fe_3O_4, $Fe_{2.33}Cr_{0.67}O_4$, $Fe_{2.09}Mn_{0.91}O_4$, $Fe_{2.10}Co_{0.90}O_4$, and $Fe_{2.06}Ni_{0.94}O_4$ labeled as M, Cr-M, Mn-M, Co-M, and Ni-M, respectively. All the samples were ground and passed through a 200 mesh screen.

The X-ray diffraction patterns (Fig. A.1) showed that all the magnetite samples had a spinel structure. However, low content of feitknechtite (JCPDS: 18-0804) was found in Mn-M. X-ray absorption fine structure (XAFS) spectra illustrated that these substituting cations entered the spinel structure. Cr^{3+}, Mn^{3+}, Co^{2+}, and Ni^{2+} mainly occupied the octahedral sites of spinel structure, while Mn^{2+} occupied the tetrahedral sites. The detailed discussion of XAFS results has been presented elsewhere (Liang et al., 2013; Zhong et al., 2013).

2.2. Surface property characterization

Specific surface area measurements were carried out by using BET method on the basis of the N_2 physical sorption capacity at 77 K on a Micromeritics ASAP 2020 instrument. All the samples were degassed at 433 K for 12 h beforehand. The surface site density (D_s) and point of zero charge (pH_{PZC}) analyses were conducted by acid-base titration method on a Mettler Toledo ET18. The test solution vessel was immersed in a thermostat controlled water bath at 25.0 ± 0.1 °C with a continuous N_2 flow to exclude CO_2. The titrations were carried out in the presence of KNO_3 as background electrolyte with different concentrations (0, 0.01, 0.05, and 0.1 mol L^{-1}). The dosages of M, Cr-M, Ni-M, Mn-M, and Co-M were 1.0, 0.25, 0.5, 1.0, and 2.0 g L^{-1}, respectively. The HNO_3 (0.1 mol L^{-1}) and KOH (0.1 mol L^{-1}) solutions were used as titrants with concentrations calibrated by Na_2CO_3 and potassium hydrogen phthalate, respectively. Initially, the pH value of magnetite suspensions was quickly lowered to 3.0 by HNO_3. After 1 h of equilibrium, the suspensions were slowly back-titrated at a constant pH increment with KOH until pH reached 11, where the additional volume of KOH (0.005–0.1 mL) was automatically adjusted to obtain the desired pH value. Each step was allowed to stabilize until the pH drift was < 0.005 pH unit min^{-1}. All solutions were prepared with preboiled deionized water and then kept under a nitrogen atmosphere to

avoid the disturbance of carbonate species. To ensure chemical equilibrium, forward (pH decrease) and reverse (pH increase) titrations should exactly overlap with no hysteresis. The PZC of the magnetite samples corresponded to the pH where the titration curves of different electrolyte concentrations intersect. The theory for acid-base titration and the calculation of D_s and pH_{PZC} can be found in the previous literature (Frini-Srasra and Srasra, 2008; Szekeres and Tombacz, 2012).

2.3. Adsorption experiment

Stock solution (500 mg L^{-1}) of Pb(II) was prepared by dissolving Pb $(NO_3)_2$ of analytical grade. The adsorption experiment was conducted at 25 °C, with the background electrolyte (KNO_3) concentration of 0, 0.01, 0.05, and 0.1 mol L^{-1}. The pH was set to 4.0, 5.0, and 6.0 and adjusted using HNO_3 (0.1 mol L^{-1}) and KOH (0.1 mol L^{-1}) solution. The initial Pb(II) concentration (C_0) was 10–160 mg L^{-1}. The dosages (m) of M, Cr-M, Ni-M, Mn-M, and Co-M were determined to be 1.0, 0.25, 0.5, 1.0, and 2.0 g L^{-1}, respectively, based on the preliminary adsorption performance to achieve similar adsorption efficiency. The suspension (V = 25 mL) was constantly stirred at RCF 13.7 for 4 h, the predetermined time for achieving adsorption equilibrium. Then, the solution samples were withdrawn and passed through a 0.22 μm PTFE filter. The residual aqueous Pb(II) concentration (C_e) was determined on a PerkinElmer (PE) AAnalyst 400 Flame Atomic Absorption Spectrophotometer with hollow-cathode lamps at a wavelength of 223.1 nm. The adsorption amount (q_e) of Pb(II) was calculated via Eq. (1):

$$q_e = (C_0 - C_e)V/m \quad (1)$$

2.4. XAFS spectroscopy

The adsorption morphology of Pb(II) on magnetite was investigated by Pb L_{III} XAFS characterization. The XAFS spectra of magnetite samples with adsorbed Pb(II) and reference compounds were measured on the beamline 1W1B of Beijing Synchrotron Radiation Facility (BSRF). The spectra were acquired at room temperature in the transmission or fluorescence mode with an ion-chamber detector filled with 100% N_2. The XAFS data were analyzed with the IFEFFIT software package (Ravel and Newville, 2005). The coordination numbers (CN), bond lengths (R), and Debye–Waller factor (σ^2) were obtained by fitting the experimental k-weighted EXAFS spectra to the standard EXAFS equation using several single-scattering paths (Kelly et al., 2008). Theoretical scattering path amplitudes and phase shifts for all the paths used in the fits were calculated using FEFF7 (Rehr et al., 1992). The passive reduction factor $S0^2$ was restrained to 0.67, which was obtained by fitting the first shell of metallic Pb foil standard. In all fits, the number of independent variables used was less than the number of independent data points. A Hanning window was used during Fourier transformation and EXAFS data fitting.

2.5. Surface complexation model

The acid-base titration and Pb(II) adsorption data were described by the diffuse layer model (DLM). The concentrations of surface sites were fixed to the maximum surface site density *Hs*. The proton affinity constant and the Pb(II) affinity constant were optimized using the computer program FITEQL 4.0. Based on XAFS characterization, a 2:3 (metal:magnetite) complexation stoichiometry was assumed for all the adsorption reaction of Pb(II) on magnetite surface. The details of the modeling procedure are summarized in Supplemental Text A.1.

3. Results and discussion

3.1. Surface properties

Surficial hydroxyl groups are essential to the surface reactions of various processes that occur at the interface between the oxide surface and an electrolyte solution. The active surface groups (≡ FeOH) at the magnetite surface are amphoteric, which can bind or release protons (Eqs. (2) and (3)) (Illes and Tombacz, 2003; Jolstera et al., 2012). Both protonation and deprotonation change the total proton concentration and surface charge density, resulting in the adsorption of cations and ligands at the metal oxide surface.

$$\equiv FeOH + H^+ \rightarrow \equiv FeOH_2^+ \quad (2)$$

$$\equiv FeOH \rightarrow \equiv FeO^- + H^+ \quad (3)$$

The total proton concentration is defined as $H_t = [H^+] - [OH^-] + [>MOH_2^+] - [>MO^-]$ and calculated from the following equation (Bujnakova et al., 2013; Nie et al., 2013):

$$H_t = (C_a V_a - C_b V_b)/(V_0 + V_a + V_b) \quad (4)$$

where C_a and C_b are the calibrated concentrations of HNO_3 and KOH, mol L^{-1}; V_0, V_a, and V_b are the volumes of the initial suspension and the consumed volumes of HNO_3 and KOH solution, repectively, L. Fig. 1a shows the acid-base titration results of pure magnetite M at different electrolyte concentrations. The surface charge density of metal oxides is affected by ionic strength; therefore, the titration curves display ionic strength dependence. The number of charged surface sites increases with increasing ionic strength (Table 1) because of the screening effect of the electrolyte (Nie et al., 2013). These characteristics are observed for magnetite M and substituted magnetites and are consistent with the previous report (Illes and Tombacz, 2003). pH_{pzc} refers to the pH value where the total net particle charge is zero. The pH_{pzc} for magnetite M is in the range of 7.35–7.48, which is stable at different electrolyte concentrations (Table 1). For the substituted magnetites, the pH_{pzc} range was 7.08–7.33 in the presence of 0.01 mol L^{-1} KNO_3, close to that of M (Fig. 1b). Among the magnetite samples, Co-M showed the most obvious buffer phenomenon in acidic pH.

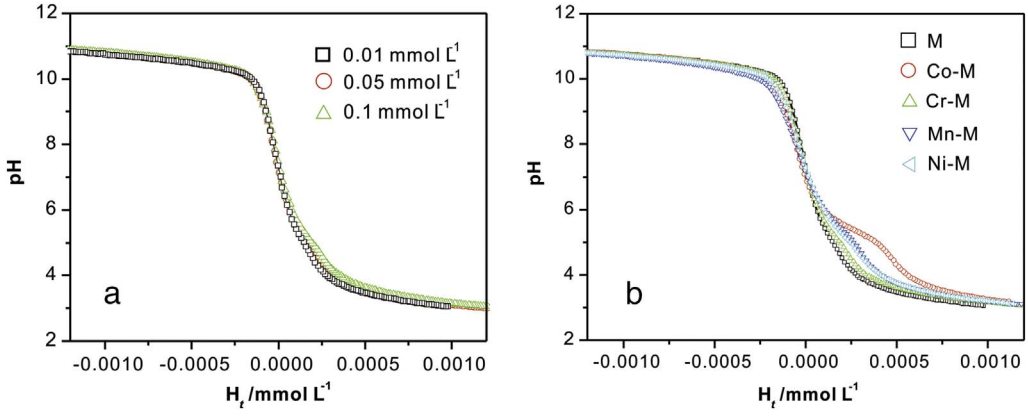

Fig. 1. Acid-base titration of magnetite nanoparticles in the KNO_3 aqueous electrolyte solutionl. a) Magnetite sample: Fe_3O_4, ionic strength: 0.01, 0.05, and 0.1 mmol L^{-1}, 25 °C; b) magnetite sample: Fe_3O_4, Co-M, Cr-M, Mn-M, and Ni-M, ionic strength: 0.01 mmol L^{-1}, 25 °C.

Table 1
The pH_{pzc} value, V_{eb1} and V_{eb2} volume for magnetite samples at different electrolyte concentrations.

Sample	KNO_3 concentration/mol L^{-1}	pH_{pzc}	$S/m^2\ g^{-1}$	[a]V_{eb1}	V_{eb2}	H_s/mol L^{-1}	D_s/sites nm^{-2}
M	0.01	7.35	28	0.476	0.533	7.07×10^{-5}	1.51
M	0.05	7.46	28	0.578	0.664	8.10×10^{-5}	1.74
M	0.1	7.48	28	0.615	0.705	8.28×10^{-5}	1.78
Co-M	0.01	7.08	9	0.411	0.58	2.64×10^{-4}	8.82
Cr-M	0.01	7.33	112	0.578	0.69	1.66×10^{-4}	3.56
Mn-M	0.01	7.20	26	0.544	0.703	2.47×10^{-4}	5.70
Ni-M	0.01	7.27	53	0.515	0.642	1.91×10^{-4}	4.35

[a] For the blank system with the presence of 0.01, 0.05 and 0.1 mol L^{-1} of KNO_3, the $V_{1\text{-blank}}$ volume is 0.617, 0.621 and 0.640, and the $V_{2\text{-blank}}$ volume is 0.633, 0.660 and 0.682 mL, respectively.

The surface site density of magnetite was determined by the Gran function (Eqs. (5)–(6)), which has been used to study the surface reactions of iron (hydr)oxides including maghemite, hematite, goethite, and ferrihydrite (Mayant et al., 2008; Jolstera et al., 2012).

$$\text{Gran} = (V_0 + V_a + V_b) \times 10^{-pH}, \text{ for pH} < 7.0 \quad (5)$$

$$\text{Gran} = (V_0 + V_a + V_b)) \times 10^{(pH + \log Kw)}, \text{ for pH} > 7.0 \quad (6)$$

K_w is the ionic product of water at given temperature and ionic strength. In this study, $\log K_w$ is considered to be -13.93 ($T = 25$ °C) (Bujnakova et al., 2013). The plot of Gran's function versus the added volume of titrant was fit with two lines that cross the X_{axis} at V_{eb1} and V_{eb2}. The titration results of M are shown in Fig. 2 as a function of the added volume of KOH solution. The V_{eb1} and V_{eb2} volumes with the presence of KNO_3 (0.01 mmol L^{-1}) were 0.476 and 0.533 mL, respectively, as determined by linear regression analysis. Both volumes increased as electrolyte concentration increased. This suggests that the KNO_3 electrolyte improves the adsorption of proton on magnetite surface.

The maximum surface proton bond site concentration H_s (mol L^{-1}) during the titration was calculated by Eq. (7). Subsequently, the surface site density D_s (site nm^{-2}) can be calculated by Eq. (8):

$$H_s = [(V_{eb2} - V_{eb1})C_b - (V_{2\text{-blank}} - V_{1\text{-blank}})C_b]/V_0 \quad (7)$$

$$D_s = (H_s N_A)/(SC_s 10^{18}) \quad (8)$$

where N_A is Avogadro's constant, 6.02×10^{23} mol^{-1}; S is the specific surface area of magnetite samples (Table 1), $m^2\ g^{-1}$; and C_s is the magnetite dosage, g L^{-1}.

D_s of M was in the range of 1.51–1.77 sites nm^{-2} and was within the D_s value reported by Tamura et al. (1993) and Sun et al. (1998), which was 1–2 sites nm^{-2}. The substitution increases D_s in the following order: Co > Mn > Ni > Cr (Table 1). Previous research has shown that there are two possible explanations for such variations. Substitution leads to the generation of crystal defects in the magnetite structure and changes the chemical composition and structure on magnetite surface. The substituting cations coordinate with hydroxyl groups by sharing the unoccupied atomic orbital to build M-OH groups, increasing the surface site density (Schwertmann and Cornell, 2008). Alternatively, ion exchange between protons and Fe(II) in the magnetite structure may increase the D_s value obtained from acidic pH titration, resulting in an overestimation of D_s. For example, some previous studies have suggested that the D_s of M is approximately 5 sites nm^{-2} (Catalette et al., 1998; Sun et al., 1998; Bujnakova et al., 2013). No acid was added during the titration; therefore, the risk of error caused by ion exchange between Fe(II) and H^+ can be neglected in this study (Jolstera et al., 2012).

3.2. Adsorption properties

3.2.1. Effect of solution pH

Pb(II) adsorption on magnetite M was tested at the solution pH of 4.0, 5.0, and 6.0 (Fig. 3). The adsorption amount was gradually enhanced as pH increased. The pH dependence effect is usually explained by the ionization of both adsorbate (Pb(II)) and adsorbent (magnetite) (Mamindy-Pajany et al., 2009). From acid-base titration, the surficial hydroxyl group on the magnetite surface was amphoteric, and protonation or deprotonation varied the surface charge. The charge can be positive, negative, or neutral, depending on the solution pH and the pH_{pzc} of magnetite M (7.35–7.48) through direct transfer of protons between the solution and mineral surface (Mamindy-Pajany et al., 2011). According to the species distribution diagram of Pb(II) as a function of pH (Fig. A.2), two species of Pb^{2+} and $Pb(OH)^+$ were predominant in the studied pH range (Bradl, 2004). The ratio of Pb^{2+}/$Pb(OH)^+$ decreased as pH increased. The surface of M was positive by protonation under the tested pH range of 4–6, which was below pH_{pzc}. The adsorption mechanism of electrostatic attraction force was not favored. As pH increased, both the ratio of Pb^{2+}/$Pb(OH)^+$ and the positive charge of magnetite surface decreased. The electrostatic repulsion

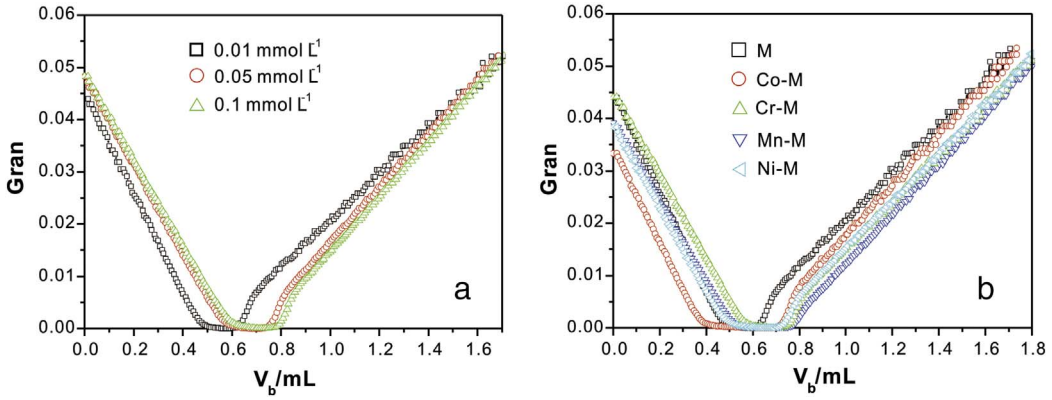

Fig. 2. Gran's plots to obtain V_1 and V_2. a) Magnetite sample: M, ionic strength: 0.01, 0.05, and 0.1 mmol L^{-1}, 25 °C; b) magnetite sample: M, Co-M, Cr-M, Mn-M, and Ni-M, ionic strength: 0.01 mmol L^{-1}, 25 °C.

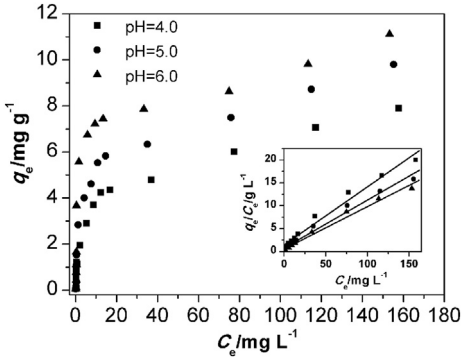

Fig. 3. Pb(II) adsorption on Fe_3O_4 at different pH. Inset: the adsorption isotherms fitted by Langmuir model. Experimental condition: Magnetite dosage = 1.0 g L^{-1}; KNO_3 concentration = 0.01 mol L^{-1}, 50 mL, 25 °C.

force was reduced, and the approach of Pb(II) near the magnetite-water interface was facilitated, resulting in improved Pb(II) adsorption. Importantly, lead hydroxide $Pb(OH)_2$ was formed at pH 6.5–13 according to the speciation distribution of Pb(II) (Fig. A.2). Therefore, the influence of Pb(II) precipitation on the removal efficiency was excluded from the studied pH range.

3.2.2. Effect of ionic strength

A substantial amount of cations and anions coexist in wastewater and the natural environment, creating potential competition for the active sites of adsorbents and prohibiting the adsorption of heavy metals (Zeng et al., 2015). An adsorption experiment was conducted at pH 5.0 by varying the KNO_3 concentration from 0.01 to 0.1 mol L^{-1} (Fig. 4) to investigate the effect of electrolyte concentration on Pb(II) adsorption by magnetite. Interestingly, the presence of electrolyte did not suppress Pb(II) adsorption. When the KNO_3 concentration increased from 0.01 to 0.05 mol L^{-1}, the Pb(II) adsorption improved, which was ascribed to the increase in surface site density (Table 1). The further increase of the KNO_3 concentration from 0.05 to 0.1 mol L^{-1} did not significantly change Pb(II) adsorption. The adsorption amount varied with the KNO_3 concentration in a similar trend to that of surface site density. The background electrolyte did not restrain the Pb(II) adsorption on magnetite. This indicates that Pb(II) had a direct chemical bond to the magnetite surface following a specific adsorption mechanism (Mamindy-Pajany et al., 2009).

3.2.3. Adsorption isotherms

From the experimental adsorption isotherms obtained at pH 5.0 and an ionic strength of 0.01 mol L^{-1} (Fig. 5), the adsorption amount q_e gradually increased as the initial concentration reached the maximum at 100 mg L^{-1}. The adsorption isotherms were analyzed by Langmuir

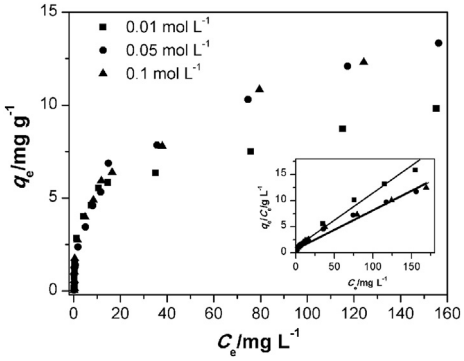

Fig. 4. Pb(II) adsorption on Fe_3O_4 at different concentration of KNO_3 electrolyte. Inset: the adsorption isotherms fitted by Langmuir model. Experimental condition: Magnetite dosage = 1.0 g L^{-1}; pH = 5.0, 50 mL, 25 °C.

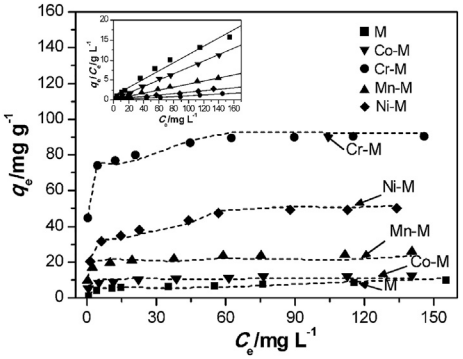

Fig. 5. Adsorption isotherms of Pb(II) by studied magnetite samples and the best fit by using the DLM model (short dash). Inset: the adsorption isotherms fitted by Langmuir model. Experimental condition: Magnetite dosage: M = 1.0 g L^{-1}, Cr-M = 0.25 g L^{-1}, Ni-M = 0.5 g L^{-1}, Mn-M = 1.0 g L^{-1}, Co-M = 2.0 g L^{-1}, pH = 5.0, KNO_3 concentration = 0.01 mol L^{-1}, 50 mL, 25 °C.

and Freundlich adsorption models (Figs. 3 and A.3) to evaluate the adsorption capacity and adsorption intensity of Pb(II) onto magnetites, and the linear forms are given by Eqs. (9) and (10), respectively (Ozmen et al., 2010). The Langmuir model assumes that adsorption takes place at specific homogeneous sites by monolayer adsorption, while the Freundlich equation models multilayer adsorption.

$$C_e/q_e = C_e/q_m + 1/q_m b \quad (9)$$

$$\log\ q_e = \log\ k + 1/n\ \log\ C_e \quad (10)$$

where q_m denotes the maximum adsorption capacity (mg g^{-1}), b is the Langmuir adsorption equilibrium constant (L mg^{-1}), and k is the Freundlich constant that roughly indicates adsorption capacity [(mg g^{-1})(mg L^{-1})$^{-1/n}$]. The value of n varies with the heterogeneity of adsorbent and for favorable adsorption processes, the n value should lie in the range of 1–10.

Correlation coefficients (R^2) suggested that the Langmuir model fit the data better (Figs. 3–5, $0.976 \le R^2 \le 0.996$) than the Freundlich model (Fig. A.3, $0.822 \le R^2 \le 0.962$). A plot of C_e/q_e vs. C_e resulted in a straight line of slope ($1/q_m$, Fig. 5). The q_m values for M, Cr-M, Mn-M, Co-M, and Ni-M were 9.8, 93.7, 26.0, 12.6, and 51.1 mg g^{-1}, respectively. The substitutions improved the adsorption capacities of magnetites towards Pb(II) in the following order: Cr > Ni > Mn > Co > M. To determine whether Pb(II) adsorption on magnetites was favorable, the isotherm shape can be classified by "R_L" as defined in Eq. (11) (Hao et al., 2010):

$$R_L = 1/(1 + bC_0) \quad (11)$$

where R_L is a dimensionless separation factor indicating an irreversible ($R_L = 0$), favorable ($0 < R_L < 1$), linear ($R_L = 1$) or unfavorable ($R_L > 1$) isotherm. The calculated R_L values in the range of 0.0012–0.56 indicated the favorable adsorption of Pb(II) on all magnetite samples and adsorption systems.

3.2.4. Adsorption geometry

Inner-sphere complexation in the monolayer was likely the dominant mechanism since the presence of background electrolyte did not suppress Pb(II) adsorption and the isotherms fit well to the Langmuir model. This adsorption mode has been found in Pb(II) adsorption on other iron (hydr)oxides such as hematite, goethite, and ferrihydrite (Bargar et al., 1997; Trivedi et al., 2003; Tiberg et al., 2013).

However, macroscopic experiments were limited to evaluation of bulk equilibrium and kinetic processes. Most adsorption mechanisms at the molecular level must be illustrated by spectroscopic characterization. For example, Komarek reported that Pb(II) adsorption on nanomaghemite was mainly via the formation of inner-sphere complexes as indicated by X-ray photoelectron spectroscopy (XPS) and X-ray

absorption fine structure (XAFS) spectroscopy (Komarek et al., 2015). Bargar et al. found that Pb(II) was adsorbed as mononuclear bidentate complexes to the edges of FeO_6 octahedra of both goethite and hematite, as confirmed by XAFS analysis (Bargar et al., 1997). Tiberg et al. reported that edge-sharing bidentate Pb(II) complexes were predominantly adsorbed on ferrihydrite (Tiberg et al., 2013). The adsorbed Pb species on Co-M and Cr-M, with the lowest and highest adsorption amounts, respectively, were characterized by XAFS to investigate the variation of adsorption geometry as the adsorption amount increased.

A comparison of the normalized XANES spectra for adsorbed Pb(II) species and selected Pb reference samples is shown in Fig. A.4. The highest absorption intensity is recorded at approximately 13.04 keV for all the samples, indicating the main valence of + 2 for the adsorbed Pb species. The spectra of Pb adsorbed on magnetites show a peak and a weak depression at approximately 13.060 and 13.094 keV, respectively. The detailed discussion of XANES results is provided in Supplemental Text A.2.

Spline-fit, *k*-weighted EXAFS spectra for magnetite samples after adsorption and selected model compounds are presented in Fig. 6a. The spectra in *k* space results from two backscattering envelopes, indicating two distinct shells surrounding the absorbed Pb(II) atoms. In the lower k-region (0.42–3.0 Å), the EXAFS oscillations are dominated by backscattering from light atoms (O) of the first coordination sphere. Intensive oscillations at high k range (3.0–8.5 Å) indicate the presence of heavy atom (Pb or Fe) in the vicinity of absorbing atoms (Xu et al., 2006; Nevidomskaya et al., 2016). The spectra for the adsorbed Pb(II) species on magnetite are even noisier in the higher-k region compared to PbO, which is attributed to the presence of highly disordered morphology (Trivedi et al., 2003).

The *k*-weighted spectra of PbO and Pb species on Cr-M and Co-M were Fourier transformed (FT) over the range of 2.3–8.9 $Å^{-1}$, and then fit over the range of 1.2–3.7 Å to reveal the geometry of Pb(II) species (Fig. 6b). Distances longer than 3.7 Å could not be fit accurately, likely due to the superposition of single and multiple scattering paths. All the FT curves mainly show two backscattering envelopes in the range of 1–3.5 Å. For PbO, two peaks appear at approximately 1.7 and 2.9 Å, which are ascribed to the Pb—O and Pb—Pb bonds, respectively. PbO contained Pb in tetrahedral coordination with the first-neighbor O, and the Pb—O distance is 2.16 Å (Nevidomskaya et al., 2016). The EXAFS analysis yielded a Pb—O distance of 2.10 Å with a coordination number (CN) of 2.7. The Pb—Pb distance in typical octahedral coordination is 3.63 Å, with a CN of 4.1. Neither spectra of absorbed Pb(II) species resemble that of PbO, which negates the possibility of surface precipitate formation. The fit of adsorbed Pb species was based on the finite ways that Pb(II) could be linked to magnetite surface. From previous studies (Trivedi et al., 2003; Tiberg et al., 2013; Huang and Pan, 2016), several adsorption configurations have been proposed for the adsorption of Pb(II) on iron oxides. For example, Pb(II) was adsorbed to the corners of FeO_6 octahedra (e.g., mononuclear/binuclear corner-sharing bidentate (Fig. 7a and b), and mononuclear monodentate (Fig. 7d)), and to the edges of FeO_6 octahedra (e.g., edge-sharing bidentate (Fig. 7c). FeO_6 octahedra in magnetite have an Fe—O bond length of approximately 2.06 Å (Liang et al., 2015). Bargar et al. reported the Pb—Fe distance of 3.49 Å for bidentate adsorption to the edges of FeO_6 octahedron, which was smaller than the Pb—Fe distance from the monodentate adsorption (4.13 Å) but larger than that of corner-sharing bidentate adsorption (3.34 Å) (Bargar et al., 1997; Trivedi et al., 2003). For a binuclear bidentate corner-sharing complex, Pb atoms also exist as second neighbor atoms with a Pb—Pb distance of 3.06 Å. The fit of a multinuclear Pb(II) surface complex was not considered because the possibility of surface precipitation was excluded.

For Pb(II) adsorbed on magnetite samples, the structural parameters derived from the best fitting of EXAFS spectra indicate the presence of three different neighboring atoms: O in the first shell and Fe and Pb atoms in the second shell (Table 2). The first shell is composed of three oxygen atoms at an average radial distance of 2.25–2.31 Å (CN = 1.8–2.3), corresponding to the backscattering at 1–2 Å on the FT curve. The first shell of highly hydrated Pb(II) ions is reported to be octahedral with radial distance for Pb—O ranging from 2.47–2.49 Å (Nevidomskaya et al., 2016). The Pb—O distance of adsorbed Pb(II) species is shorter than that of hydrated Pb(II) ions, suggesting that Pb (II) cations do not retain their hydration sphere after the adsorption on magnetite. The Pb—O radial distance is also smaller than the Pb—O bond in $PbCO_3$ (2.69 Å), $Pb(OH)_2$ (2.32 Å), and lead oxides (2.40 Å) in agreement with the absence of surface precipitation.

Although only one backscattering is observed at 2.2–3.4 Å, the second shell is best fitt with one Pb atom and two Fe atoms. The fitted Pb—Pb (CN = 0.67 ± 0.10) and Pb—Fe (CN = 1.34 ± 0.20) distances are 3.02 and 3.32 Å, respectively. The presence of Pb atoms in the second shell indicates binuclear geometry. The fitted Pb—Fe distance is close to that in the corner-sharing bidentate complex. This illustrates that Pb(II) adsorption on magnetite has bidentate binuclear geometry. For Cr-M and Co-M, the CN and distances for Pb—O, Pb—Pb and Pb—Fe are similar. This indicates that adsorption geometry does not vary with the increase in adsorption capacity.

3.3. Surface-adsorption relationship

In this study, Pb(II) was adsorbed on the magnetite surface by forming inner-sphere complexes. Metals act as a Lewis acid (i.e., an electron acceptor) in aqueous solution. The electron-pair donating surface groups (e.g., –OH, − SH, and –COOH) and metal cations form Lewis salt-type compounds (Bradl, 2004). Under the studied condition, Pb(II) was in the form of Pb^{2+}, and $Pb(OH)^{+}$ acting as a Lewis acid, while the hydroxyl group on the magnetite surface acted as Lewis basis (≡ FeOH) to bind Pb(II) and form bidentate binuclear complexes (Eq.

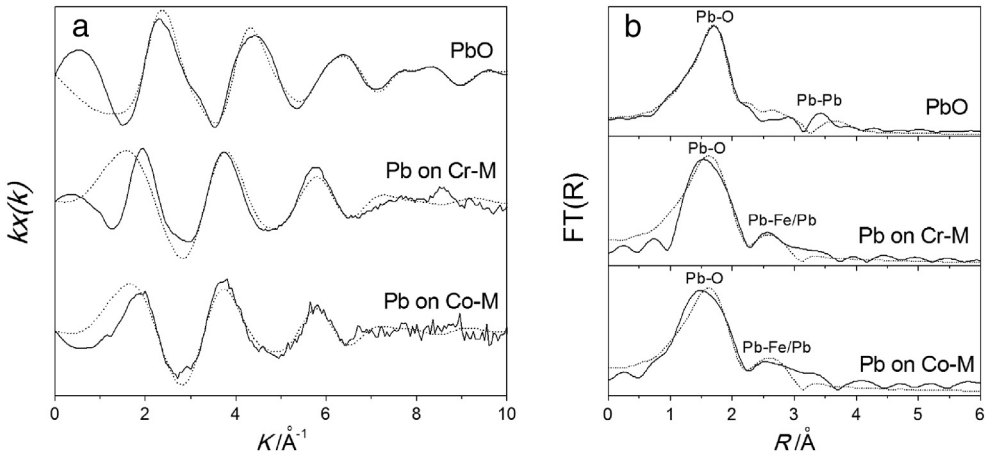

Fig. 6. (a) Pb-L_{III}-edge EXAFS spectra of Pb(II) adsorbed on Cr-M and Co-M magnetites and the reference sample PbO. (b) fourier transforms (FTs) uncorrected for phase shift. Fourier transform limits were from k = 1.1 $Å^{-1}$ to k = 8.5–10 $Å^{-1}$. For each EXAFS spectrum, and FT, the line of zero amplitude is given by the corresponding horizontal line.

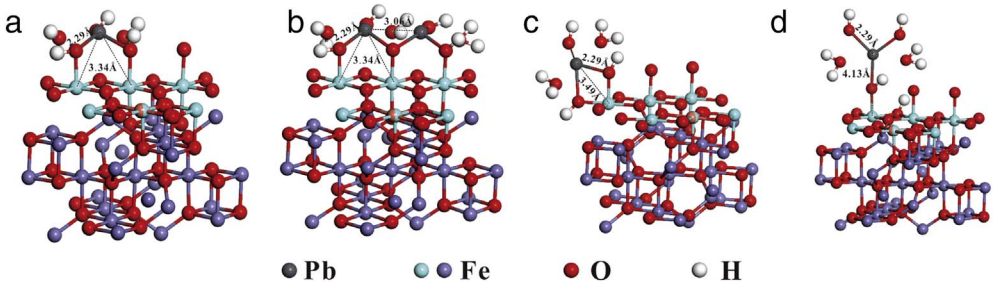

Fig. 7. Schematic representations of the predominated Pb(II)-iron oxides adsorption complexes based on previous literature. a) Bidentate mononuclear corner-sharing complex; b) bidentate binuclear corner-sharing complex; c) monodentate complex; d) bidentate edge-sharing complex.

(12)). Based on the XAFS characterization, the adsorption geometry was not varied as the adsorption capacity increased.

$$3(\equiv FeOH) + 2Pb^{2+} + 2H_2O \rightarrow (\equiv Fe_3O_2OHPb_2(OH)_2)^0 + 3H^+ \quad (12)$$

Based on the stoichiometry of 3:2 between the ≡FeOH group and adsorbed Pb(II) cations, the active site density (D_{cal}, sites nm^{-2}) on the magnetite surface could be calculated by Eq. (13):

$$D_{cal} = 1.5 q_m N_A / (SM_{Pb} 10^{18}) \quad (13)$$

where N_A is the Avogadro constant (6.02×10^{23}), S is the specific surface area of magnetite samples (Table 1), and M_{Pb} is the molar mass of Pb (207.2 g mol^{-1}). The calculated D_{cal} values for M, Cr-M, Mn-M, Co-M, and Ni-M were 1.53, 3.65, 4.36, 6.15, and 4.20 sites nm^{-2}, respectively. D_{cal} was comparable to D_s, which was determined by acid-base titration (Table 1 and Fig. 8). A linear relationship between D_{cal} and D_s was observed, indicating the vital role of active site density in Pb (II) adsorption on magnetite. Among most magnetite samples, especially for M, Cr-M, and Ni-M, D_{cal} is close to D_s. This confirms the dominant adsorption geometry was bidentate binuclear corner-sharing for Pb(II) adsorbed on the magnetite surface.

3.4. Surface complexation model

The adsorption isotherms of Pb(II) on magnetite with substitutions were simulated by the DLM modeling. Based on the EXAFS analysis, the inner-sphere surface complexation dominates the adsorption of Pb(II) on magnetite (Eq. (12)). Therefore, the bidentate binuclear complex species $\equiv Fe_3O_2OHPb_2^{2+}$ was employed in magnetite systems. The isothermal adsorption data of Pb(II) on all the magnetite samples was satisfactorily fit at low ionic strength of 0.01 mol L^{-1} (Fig. 5). The obtained surface affinity constants ($logK_{Mag\text{-}Pb}$) were in the range of 11.9–14.4 (Table 3). However, at high ionic strength, e.g., 0.05 and 0.1 mol L^{-1}, the adsorption amount on M sample was overestimated by the DLM, especially at high Pb(II) concentration (Fig. A.7). This was probably ascribed to the compression of electric double layer (Csoban and Joo, 1999). Besides, the activity of surficial hydroxyl sites on M sample surface did not change with the ionic strength increase and the competition of the background electrolyte cation (i.e., K^+) for deprotonated site at high ionic strength could be ignored (Table 3) (Borrok and Fein, 2005). Attempts were also made to simulate the experimental data after the introduction of other complexes with stoichiometry of 2:1 and 1:1 (Fig. 7a, c and d), but the fitting quality was inferior to that of $(\equiv Fe_3O_2OHPb_2(OH)_2)^0$ complexes. The results of surface complexation modeling indicates that Pb(II) was adsorbed on magnetite through the formation of $(\equiv Fe_3O_2OHPb_2(OH)_2)^0$ complexes.

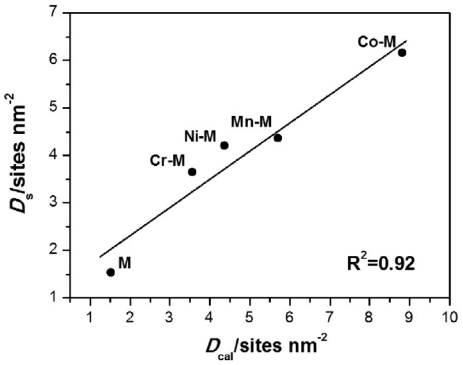

Fig. 8. Relationship between the calculated active site density (D_{cal}) by the adsorbed amount and the determined active site density (D_s) by acid-base titration.

Table 3
The proton affinity constant and the Pb(II) affinity constant of magnetite with different substitutions.

Sample	Ionic strength/mmol L^{-1}	$logK_{FeOH2+}$	$logK_{FeO-}$	$logK_{Mag\text{-}Pb}$
M	0.01–0.1	7.45	−4.59	13.78
Co-M	0.01	8.8	−8.4	11.92
Cr-M	0.01	7.68	−8.76	13.54
Mn-M	0.01	9.29	−7.84	14.43
Ni-M	0.01	8.67	−7.47	14.45

$logK_{FeOH2+}$: protonation constant of surface hydroxyl groups; $logK_{FeO-}$: deprotonation constant of surface hydroxyl groups; $logK_{Mag\text{-}Pb}$: Pb(II) affinity constant.

4. Conclusion

In this study, the adsorption of Pb(II) on magnetites substituted by the transition metals Cr, Mn, Co, and Ni, was investigated through a combination of batch adsorption experiment, XAFS investigation and DLM modeling. The substitutions in magnetite varied the surface site density and specific surface area, but pH_{PZC} did not change obviously.

Table 2
Results of EXAFS analyses (CN = coordination number, R = interatomic distance, and σ^2 = Debye-Waller factor).

Sample	Pb-O			Pb-Pb			Pb-Fe		
	CN	R(Å)	σ^2	CN	R(Å)	σ^2	CN	R(Å)	σ^2
PbO	2.7(3)	2.19(3)	0.004	4.1	3.63	0.011			
(R = 0.018)	(0.3)	(0.03)		(0.5)	(0.13)				
Pb on Cr-M	2.1	2.29	0.012	0.67	2.92	0.015	1.34	3.33	0.023
(R = 0.020)	(0.2)	(0.04)		(0.1)	(0.05)		(0.2)	(0.14)	
Pb on Co-M	2.0	2.28	0.013	0.67	3.02	0.014	1.34	3.33	0.020
(R = 0.019)	(0.2)	(0.04)		(0.1)	(0.06)		(0.2)	(0.14)	

The substitution increased the Pb(II) adsorption capacity. Based on the adsorption capacity and geometry, the reacted active site density was calculated and was found to be close to that determined by acid-base titration. The specific adsorption mechanism and vital role of the hydroxyl active group were indicated by this result. Our results showed that the substitutions changed the surface physiochemistry properties of magnetite, resulting in the variation of adsorption capacity towards Pb (II). Pb(II) was fixed on the magnetite surface by the formation of bidentate binuclear inner-sphere complexes.

The crust of the earth consists of rocks, which are the primary sources of magnetite and supply most of the iron cycled through the earth's surface ecosystems. Among the three basic groups of rocks (i.e., magmatic, metamorphic and sedimentary), magmatic rocks cover most of the solid earth surface, in which the major Fe oxides are magnetite and ilmenite, and to a lesser extent, hematite. Thus, magmatic magnetite is vital to the transport and transformation of contaminants. In contrast to biogenic magnetite and neoformed magnetite, magmatic magnetite has extensive isomorphous substitution (e.g., Cr^{3+} for Fe^{3+}; Mn^{2+}, Co^{2+}, and Ni^{2+} for Fe^{3+}) in its structure. Most of these substitutions enhance the adsorption capacities of Pb(II) on magnetite surface. This suggests that Pb(II) cannot be transported easily within the environment in the presence of magnetite. This study is significant for understanding the adsorption mechanism of Pb(II) on nano-sized magnetite and the fate of toxic metals in the aquatic and soil environment.

Acknowledgement

This work was financially supported by the National Key R & D Program of China (Grant No. 2016YFD0800704), the National Natural Science Foundation of China (Grant Nos. 41302026 and 41572032), Science and Technology Program of Guangzhou, China (Grant No. 201607010236), Youth Innovation Promotion Association CAS (Grant No. 2014324), Newton Advanced Fellowship (Grant No. NA150190) and CAS/SAFEA International Partnership Program for Creative Research Teams (Grant No. 20140491534). We would like to thank Beijing Synchrotron Radiation Facility (BSRF) for giving us the beam time for the XAFS measurement. This is contribution No.IS-2432 from GIGCAS.

Appendix A. Supplementary data

Supplementary information for surface complexation model and XANES result discussion, as well as the supplementary data for the characterization results of XRD, species distribution of Pb(II), adsorption isotherms fitted by Freundlich and XANES spectra of adsorbed Pb (II) on magnetite and reference samples, can be found in the online version at http://dx.doi.org/10.1016/j.chemgeo.2017.09.003.

References

Arce, V.B., et al., 2015. EXAFS and DFT study of the cadmium and lead adsorption on modified silica nanoparticles. Spectrochim. Acta A 151, 156–163.
Bargar, J.R., Brown, G.E., Parks, G.A., 1997. Surface complexation of Pb(II) at oxide-water interfaces.2. XAFS and bond-valence determination of mononuclear Pb(II) sorption products and surface functional groups on iron oxides. Geochim. Cosmochim. Acta 61 (13), 2639–2652.
Bargar, J.R., Brown, G.E., Parks, G.A., 1998. Surface complexation of Pb(II) at oxide-water interfaces: III. XAFS determination of Pb(II) and Pb(II)-chloro adsorption complexes on goethite and alumina. Geochim. Cosmochim. Acta 62 (2), 193–207.
Borrok, D.M., Fein, J.B., 2005. The impact of ionic strength on the adsorption of protons, Pb, Cd, and Sr onto the surfaces of Gram negative bacteria: testing non-electro static, diffuse, and triple-layer models. J. Colloid Interface Sci. 286 (1), 110–126.
Bradl, H.B., 2004. Adsorption of heavy metal ions on soils and soils constituents. J. Colloid Interface Sci. 277 (1), 1–18.
Bujnakova, Z., et al., 2013. Arsenic sorption by nanocrystalline magnetite: an example of environmentally promising interface with geosphere. J. Hazard. Mater. 262, 1204–1212.
Catalette, H., Dumonceau, J., Ollar, P., 1998. Sorption of cesium, barium and europium on magnetite. J. Contam. Hydrol. 35 (1–3), 151–159.
Christophi, C.A., Axe, L., 2000. Competition of Cd, Cu, and Pb adsorption on goethite. J. Environ. Eng. ASCE 126 (1), 66–74.
Coston, J.A., Fuller, C.C., Davis, J.A., 1995. Pb^{2+} and Zn^{2+} adsorption by a natural aluminum-bearing and iron-bearing surface coating on an aquifer sand. Geochim. Cosmochim. Acta 59 (17), 3535–3547.
Csoban, K., Joo, P., 1999. Sorption of Cr(III) on silica and aluminium oxide: experiments and modelling. Colloids Surf. A Physicochem. Eng. Asp. 151 (1–2), 97–112.
Eick, M.J., Peak, J.D., Brady, P.V., Pesek, J.D., 1999. Kinetics of lead adsorption/desorption on goethite: residence time effect. Soil Sci. 164 (1), 28–39.
Elzinga, E.J., Peak, D., Sparks, D.L., 2001. Spectroscopic studies of Pb(II)-sulfate interactions at the goethite-water interface. Geochim. Cosmochim. Acta 65 (14), 2219–2230.
Filip, J., et al., 2014. Anaerobic reaction of nanoscale zerovalent iron with water: mechanism and kinetics. J. Phys. Chem. C 118 (25), 13817–13825.
Frini-Srasra, N., Srasra, E., 2008. Determination of acid-base properties of HCl acid activated palygorskite by potentiometric titration. Surf. Eng. Appl. Electrochem. 44 (5), 401–409.
Gorski, C.A., Nurmi, J.T., Tratnyek, P.G., Hofstetter, T.B., Scherer, M.M., 2010. Redox behavior of magnetite: implications for contaminant reduction. Environ. Sci. Technol. 44 (1), 55–60.
Hao, Y.M., Chen, M., Hu, Z.B., 2010. Effective removal of Cu(II) ions from aqueous solution by amino-functionalized magnetic nanoparticles. J. Hazard. Mater. 184 (1–3), 392–399.
Huang, X.M., Pan, M., 2016. The highly efficient adsorption of Pb(II) on graphene oxides: a process combined by batch experiments and modeling techniques. J. Mol. Liq. 215, 410–416.
Illes, E., Tombacz, E., 2003. The role of variable surface charge and surface complexation in the adsorption of humic acid on magnetite. Colloids Surf. A Physicochem. Eng. Asp. 230 (1–3), 99–109.
Jolstera, R., Gunneriusson, L., Holmgren, A., 2012. Surface complexation modeling of Fe_3O_4-H^+ and magnesium(II) sorption onto maghemite and magnetite. J. Colloid Interface Sci. 386, 260–267.
Kelly, M.J., Kim, J., Roberts, G.W., Lamb, H.H., 2008. Characterization of Pd/γ-Al_2O_3 catalysts prepared using [Pd(hfac)$_2$] in liquid CO_2. Top. Catal. 49 (3–4), 178–186.
Komarek, M., Koretsky, C.M., Stephen, K.J., Alessi, D.S., Chrastny, V., 2015. Competitive adsorption of Cd(II), Cr(VI), and Pb(II) onto nanomaghemite: a spectroscopic and modeling approach. Environ. Sci. Technol. 49 (21), 12851–12859.
Liang, X.L., et al., 2013. The valence and site occupancy of substituting metals in magnetite spinel structure $Fe_{3-x}M_xO_4$ (M = Cr, Mn, Co and Ni) and their influence on thermal stability: an XANES and TG-DSC investigation. Solid State Sci. 15, 115–122.
Liang, X.L., et al., 2014. The distinct effects of Mn substitution on the reactivity of magnetite in heterogeneous Fenton reaction and Pb(II) adsorption. J. Colloid Interface Sci. 426, 181–189.
Liang, X.L., et al., 2015. The oxidation state and microstructural environment of transition metals (V, Co, and Ni) in magnetite: an XAFS study. Phys. Chem. Miner. 42 (5), 373–383.
Ma, S.C., Zhang, J.L., Sun, D.H., Liu, G.X., 2015. Surface complexation modeling calculation of Pb(II) adsorption onto the calcined diatomite. Appl. Surf. Sci. 359, 48–54.
Mamindy-Pajany, Y., Hurel, C., Marmier, N., Roméo, M., 2009. Arsenic adsorption onto hematite and goethite. C. R. Chim. 12 (8), 876–881.
Mamindy-Pajany, Y., Hurel, C., Marmier, N., Romeo, M., 2011. Arsenic (V) adsorption from aqueous solution onto goethite, hematite, magnetite and zero-valent iron: effects of pH, concentration and reversibility. Desalination 281, 93–99.
Mason, S.E., Iceman, C.R., Tanwar, K.S., Trainor, T.P., Chaka, A.M., 2009. Pb(II) adsorption on isostructural hydrated alumina and hematite (0001) surfaces: a DFT study. J. Phys. Chem. C 113 (6), 2159–2170.
Mayant, C., Grambow, B., Abdelouas, A., Ribet, S., Ledercq, S., 2008. Surface site density, silicic acid retention and transport properties of compacted magnetite powder. Phys. Chem. Earth 33 (14–16), 991–999.
Nevidomskaya, D.G., et al., 2016. Comprehensive study of Pb (II) speciation in soil by X-ray absorption spectroscopy (XANES and EXAFS) and sequential fractionation. J. Soils Sediments 16 (4), 1183–1192.
Nie, G.Z., Pan, B.C., Zhang, S.J., Pan, B.J., 2013. Surface chemistry of nanosized hydrated ferric oxide encapsulated inside porous polymer: modeling and experimental studies. J. Phys. Chem. C 117 (12), 6201–6209.
Orsetti, S., Quiroga, M.D.L.M., Andrade, E.M., 2006. Binding of Pb(II) in the system humic acid/goethite at acidic pH. Chemosphere 65 (11), 2313–2321.
Ozmen, M., et al., 2010. Adsorption of Cu(II) from aqueous solution by using modified Fe_3O_4 magnetic nanoparticles. Desalination 254 (1–3), 162–169.
Perelomov, L., Cozzolino, V., Pigna, M., Violante, A., 2011. Adsorption of Cu and Pb on goethite in the presence of low-molecular mass aliphatic acids. Geomicrobiol J. 28 (7), 582–589.
Ravel, B., Newville, M., 2005. ATHENA, ARTEMIS, HEPHAESTUS: data analysis for X-ray absorption spectroscopy using IFEFFIT. J. Synchrotron Radiat. 12, 537–541.
Rehr, J.J., Albers, R.C., Zabinsky, S.I., 1992. High-order multiple-scattering calculations of X-ray absorption fine structure. Phys. Rev. Lett. 69 (23), 3397–3400.
Reich, T.J., Das, S., Koretsky, C.M., Lund, T.J., Landry, C.J., 2010. Surface complexation modeling of Pb(II) adsorption on mixtures of hydrous ferric oxide, quartz and kaolinite. Chem. Geol. 275 (3–4), 262–271.
Schwertmann, U., Cornell, R.M., 2008. Iron Oxides in the Laboratory: Preparation and Characterization. John Wiley & Sons, Federal Republic of Germany.
Scott, T.B., Allen, G.C., Heard, P.J., Randell, M.G., 2005. Reduction of U(VI) to U(IV) on the surface of magnetite. Geochim. Cosmochim. Acta 69 (24), 5639–5646.
Sun, Z.X., Su, F.W., Forsling, W., Samskog, P.O., 1998. Surface characteristics of magnetite in aqueous suspension. J. Colloid Interface Sci. 197 (1), 151–159.
Szekeres, M., Tombacz, E., 2012. Surface charge characterization of metal oxides by

potentiometric acid-base titration, revisited theory and experiment. Colloids Surf. A Physicochem. Eng. Asp. 414, 302–313.
Tamura, H., Katayama, N., Furuichi, R., 1993. Modeling the ion-exchange adsorption of heavy-metal ions on the surface of metal-oxides. Bunseki Kagaku 42 (11), 719–724.
Templeton, A.S., Spormann, A.M., Brown, G.E., 2003. Speciation of Pb(II) sorbed by Burkholderia cepacia/goethite composites. Environ. Sci. Technol. 37 (10), 2166–2172.
Tiberg, C., Sjostedt, C., Persson, I., Gustafsson, J.P., 2013. Phosphate effects on copper(II) and lead(II) sorption to ferrihydrite. Geochim. Cosmochim. Acta 120, 140–157.
Trivedi, P., Dyer, J.A., Sparks, D.L., 2003. Lead sorption onto ferrihydrite. 1. A macroscopic and spectroscopic assessment. Environ. Sci. Technol. 37 (5), 908–914.
Villalobos, M., Perez-Gallegos, A., 2008. Goethite surface reactivity: a macroscopic investigation unifying proton, chromate, carbonate, and lead(II) adsorption. J. Colloid Interface Sci. 326 (2), 307–323.
Villalobos, M., Trotz, M.A., Leckie, J.O., 2001. Surface complexation modeling of carbonate effects on the adsorption of Cr(VI), Pb(II), and U(VI) on goethite. Environ. Sci. Technol. 35 (19), 3849–3856.
Wang, X.S., Lu, H.J., Zhu, L., Liu, F., Ren, J.J., 2010. Adsorption of lead(II) ions onto magnetite nanoparticles. Adsorpt. Sci. Technol. 28 (5), 407–417.
Wei, G.L., et al., 2015. Heterogeneous activation of Oxone by substituted magnetites $Fe_{3-x}M_xO_4$ (Cr, Mn, Co, Ni) for degradation of Acid Orange II at neutral pH. J. Mol. Catal. A Chem. 398, 86–94.
Wiatrowski, H.A., et al., 2009. Reduction of Hg(II) to Hg(O) by magnetite. Environ. Sci. Technol. 43 (14), 5307–5313.
Xu, Y., Boonfueng, T., Axe, L., Maeng, S., Tyson, T., 2006. Surface complexation of Pb(II) on amorphous iron oxide and manganese oxide: spectroscopic and time studies. J. Colloid Interface Sci. 299 (1), 28–40.
Zeng, G.M., et al., 2015. Enhancement of Cd(II) adsorption by polyacrylic acid modified magnetic mesoporous carbon. Chem. Eng. J. 259, 153–160.
Zhang, M.Y., Pan, G., Zhao, D.Y., He, G.Z., 2011. XAFS study of starch-stabilized magnetite nanoparticles and surface speciation of arsenate. Environ. Pollut. 159 (12), 3509–3514.
Zhang, J.H., et al., 2017. Reduction removal of hexavalent chromium by zinc-substituted magnetite coupled with aqueous Fe(II) at neutral pH value. J. Colloid Interface Sci. 500, 20–29.
Zhao, D.L., Chen, C.L., Sheng, G.D., Wang, X.K., 2011. Effect of environmental conditions on the retention behaviour of Pb(II) by hematite. J. Chem. Technol. Biotechnol. 86 (8), 1099–1106.
Zhong, Y.H., et al., 2013. A comparative study about the effects of isomorphous substitution of transition metals (Ti, Cr, Mn, Co and Ni) on the UV/Fenton catalytic activity of magnetite. J. Mol. Catal. A Chem. 372, 29–34.